



# Mid-infrared hybrid Si/VO<sub>2</sub> modulator electrically driven by graphene electrodes

MEHDI SADEGHI,<sup>1</sup> BABAK JANJAN,<sup>1,3</sup> MOHSEN HEIDARI,<sup>1,4</sup>  AND DEREK ABBOTT<sup>2</sup>

<sup>1</sup>Department of Electrical Engineering, Tarbiat Modares University, 14115-116 Tehran, Iran

<sup>2</sup>School of Electrical & Electronic Engineering, University of Adelaide, SA 5005, Australia

<sup>3</sup>b.janjan@modares.ac.ir

<sup>4</sup>mh.heidari@modares.ac.ir

**Abstract:** Silicon photonic platforms are of significant interest for a variety of applications that operate in the mid-infrared regime. However, the realization of efficient mid-IR modulators, key components in any integrated optics platform, is still a challenging topic. Here, an ultra-compact high-speed hybrid Si/VO<sub>2</sub> modulator operating at a mid-IR wavelength of 3.8  $\mu\text{m}$  is presented. Electrical properties of graphene are employed to achieve a reversible insulating-metal phase transition in VO<sub>2</sub> by electrical actuation. The thermal characteristics of graphene are employed to improve the response time of the VO<sub>2</sub> phase transition through speed up heating and dissipation processes, thus enhancing the modulation speed. Optical and thermal simulations show an extinction ratio of 4.4 dB/ $\mu\text{m}$ , an insertion loss of 0.1 dB/ $\mu\text{m}$ , and high modulation speed of 23 ns. A larger modulation depth as high as 10 dB/ $\mu\text{m}$  can be achieved at the cost of lower modulation speed.

© 2020 Optical Society of America under the terms of the [OSA Open Access Publishing Agreement](#)

## 1. Introduction

After significant development in the near-infrared (IR) region for more than two decades, silicon photonics is of great interest for realizing mid-IR photonic integrated circuits due to its unique properties such as low loss and compatibility with CMOS technology. In the mid-IR regime, there are a large number of potential applications including thermal imaging, medical diagnostics and gas sensing [1–4]. However, due to the lattice symmetry of silicon, the material does not exhibit a second-order susceptibility that is essential for realizing an optical modulator as a key building block for a wide variety of applications [5–7]. Alternative approaches for realizing optical modulators rely on the thermo-optic effect [8] and the free-carrier dispersion (FCD) effect [6,9,10]. However, these effects are relatively weak, and consequently, the corresponding modulators require a large footprint and high energy consumption to reach reasonable modulation performance that limits applications in silicon photonics. Although resonance-based structures can be employed to reduce the footprint and energy consumption, they suffer from narrow optical bandwidth and limited temperature tolerance [11,12]. These limitations motivate the need to combine efficient active materials with silicon photonics to form a hybrid structure mixing the properties of the incorporated material and silicon.

Among several materials under study, VO<sub>2</sub> stands out due to its unique properties [13]. First, it is compatible with the standard CMOS fabrication process that facilitates the integration of VO<sub>2</sub> with silicon photonics and electronic devices and hence the realization of silicon optoelectronic integrated systems. Second, VO<sub>2</sub> is a phase change material exhibiting a reversible insulator-metal phase transition that provides a huge refractive index change of  $\Delta n > 1$  and  $\Delta \kappa \approx$  order of magnitude [14–16]. This refractive index change is orders of magnitude larger than that of pure silicon photonic devices based on FCD or thermo-optic effect. It is therefore possible to diminish the footprint of hybrid silicon modulators by orders of magnitude compared to that of pure silicon. Nowadays, many different types of hybrid Si/VO<sub>2</sub> optical modulators operating in

the near-IR band have been already proposed [16–19]. However, the main notable challenge of VO<sub>2</sub>-based optical modulators is the relatively low phase transition speed of the VO<sub>2</sub> that limits the maximum achievable modulation speed. This restricts the application of VO<sub>2</sub>-based optical modulator to the sub-Gbps range.

For triggering VO<sub>2</sub> electrically, the insulating to conducting phase transition can occur within the first tens of nanoseconds while the reverse transition from conducting to insulating is a slower process, thus limiting switching time of VO<sub>2</sub> [20]. This is mainly because due to the weak thermal conductivity of the structure, the heat dissipation rate of devices is limited, and thus the VO<sub>2</sub> returns to the conducting phase with significant delay. Although current-limiting resistance [20] and dual-polarization four-level pulse amplitude modulation [19] are suggested to improve the speed limitation of the VO<sub>2</sub> phase transition, the latter has the drawback of complexity in structure and fabrication and the former has the drawback of poor extinction ratio. Therefore, a viable solution to overcome this limitation remains the main challenging in the designation of high speed VO<sub>2</sub>-based optical modulators and other active devices.

Graphene, a 2D material consisting of carbon atoms arranged in a hexagonal lattice, has been widely used in silicon photonics devices owing to many unique properties [21–25]. In particular, it has the highest thermal conductivity up to 5300 W/mK among all known materials [26]. It has been reported that the use of graphene as a microheater can significantly reduce the response time of thermo-optic Si modulators relative to devices without graphene [27,28]. To this point, the combination of graphene sheet with VO<sub>2</sub>-based modulators can significantly help to achieve a high heat transfer rate in a device. This ensures the heat of VO<sub>2</sub> dissipates at high speed which reduces the recovery time of VO<sub>2</sub> transition and improves the modulation speed. Shrinking the volume of active VO<sub>2</sub> also can aid to reach lower response time. However, the reduction of active VO<sub>2</sub> volume leads to a reduction of modulation performance such as extinction ratio. To overcome this problem, an embedded VO<sub>2</sub> layer in vertical silicon slot waveguide is employed to enhance the interaction between VO<sub>2</sub> and light [17].

In this paper, a high speed ultra-compact mid-IR silicon modulator based on VO<sub>2</sub> material and electrically triggered with graphene electrodes is proposed. The VO<sub>2</sub> material is embedded in a vertical silicon slot waveguide in order to shrink the volume of VO<sub>2</sub> while maintaining the high performance of the modulator. The thin embedded VO<sub>2</sub> layer leads an increase in the heating process while the graphene electrodes help to speed up the heat dissipation in VO<sub>2</sub> material and as a result the response time of reverse phase transition is significantly reduced. Our simulation results show a theoretical modulation speed below 23 ns and an extinction ratio of 4.4 dB/μm with insertion loss of lower than 0.1 dB/μm near mid-IR wavelength of  $\lambda = 3.8 \mu\text{m}$ . Also, 10 dB/μm extinction ratio can be obtained by sacrificing the modulation speed.

The rest of this paper is organized as follows: the structure of the electrical triggered VO<sub>2</sub> by graphene electrodes and the modulation behavior are described in Section 2. Then the performance of the proposed modulator in term of extinction ratio, insertion loss, and wavelength dependency calculated by using three-dimensional FDTD simulation, and compared against the results of the previously reported devices in the same section are investigated in Section 3. Thermal simulations to show the superior benefit of graphene electrodes in the improving modulation speed are also conducted in this section. Finally, a brief summary of the results and the concluding remarks are provided in Section 4.

## 2. The proposed structure

The perspective and cross-sectional view of the proposed hybrid Si/VO<sub>2</sub> mid-IR modulator are shown in Fig. 1. It consists of a silicon-graphene-VO<sub>2</sub>-graphene-silicon vertical stack layer that is inserted into a silicon waveguide. To realize the device, the lower silicon rail is buried in the SiO<sub>2</sub> substrate. Electrical signals are applied on the VO<sub>2</sub> layer by two graphene sheets contacted via two Ti/Au electrodes that are placed sufficiently far from the waveguide core to avoid mode

disturbance induced by metal. A Ti adhesion layer between graphene and Au is considered to reduce the Au/graphene contact resistance [29].

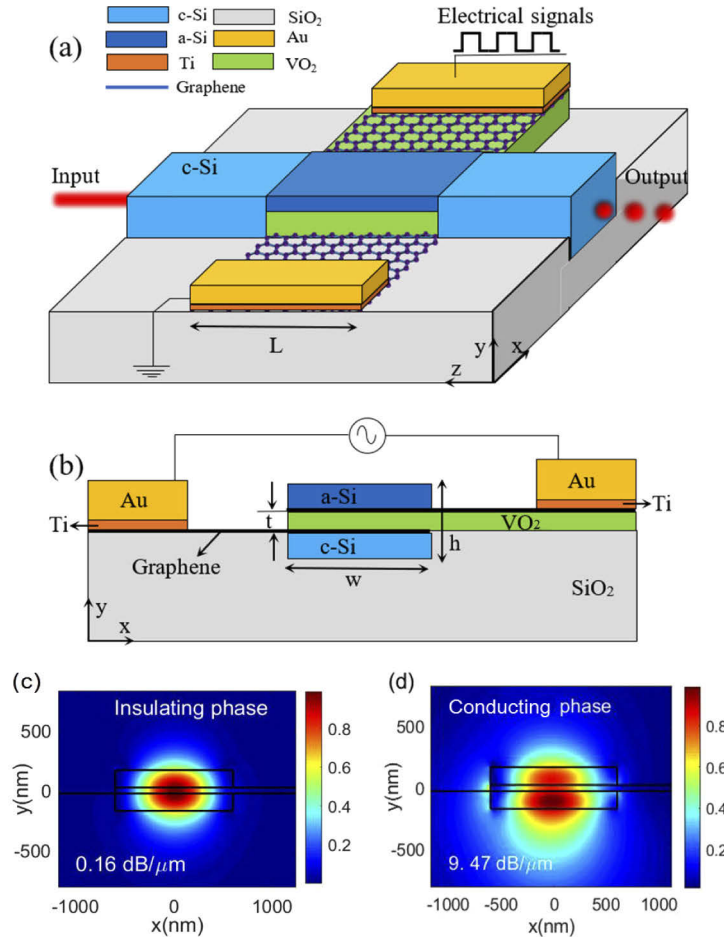


**Fig. 1.** (a) Perspective view and (b) cross-sectional view of the proposed hybrid Si/VO<sub>2</sub> modulator. The power distribution profile of excited optical mode in hybrid Si/VO<sub>2</sub> waveguide when the VO<sub>2</sub> is in the (c) insulating and (d) conducting phase.

An input silicon waveguide with a cross-section of  $w \times h = 1.2 \times 0.34 \mu\text{m}^2$  is designed to ensure that only fundamental quasi-TE mode is well-guided at a mid-IR wavelength of  $\lambda = 3.8 \mu\text{m}$ . Single-mode operation prevents multi-mode interference that distorts the spectrum of the device. According to the cross-section of the device shown in Fig. 1(b), the thickness and the length of the VO<sub>2</sub> layer are  $t$  and  $L$ , respectively. The optical properties of the material incorporating the device at the central wavelength  $\lambda = 3.8 \mu\text{m}$  are listed in Table 1. Also, in our optical simulation, graphene material is modeled as a surface conductivity layer characterized by the Kubo formula [30], and it depends on Fermi energy level  $E_F$ , the operating frequency  $\omega$ , carrier scattering time  $\tau$ , and the temperature  $T$ . In what follows, we choose  $E_F = 0.5 \text{ eV}$  and  $\tau = 0.5 \text{ ps}$ . The wavelength dispersion of the refractive index is also taken into account in our simulations.

The optical performance of the proposed structure is simulated using FDTD-based commercial software Lumerical FDTD Solutions with an auto non-uniform meshing accuracy of 8 and perfectly matched layer boundary conditions, which are sufficiently far away from the modeled

**Table 1. Material Properties.**

Material	Refractive index	Density (kg/m <sup>3</sup> )	C <sub>p</sub> (J/kgK)	Thermal conductivity (W/mK)
VO <sub>2</sub> (Insulating) [31–33]	2.71+0.08i	4571	656	3.5
VO <sub>2</sub> (Conducting) [31–33]	4.05+5.32i	4653	757	5.5
c-Silicon [34]	3.43	2300	700	148
a-Silicon [34,35]	3.82	2285	992	1.5
SiO <sub>2</sub> [34]	1.40	2203	703	1.38
Graphene [36]	-	2267	2082	3000

structure to avoid their disturbance on the results. The input power is launched to the device by exciting the fundamental quasi-TE mode of the silicon waveguide and frequency-domain field and power monitors are employed to collect the power reaching the end of the device at silicon waveguide. Therefore, the coupling loss between the silicon waveguide and the proposed modulator originating from their field profile mismatch are included in our results. This device has two working states depending upon applied voltage pulse, ON- (voltage is ON) and OFF- (voltage is OFF) states. In the OFF-state, VO<sub>2</sub> is in the insulating state and has relatively high refractive index of 2.71 ( $n_{Si} = 3.43$ ). Considering thin thickness of the embedded VO<sub>2</sub> layer, this causes mode profile of hybrid Si/VO<sub>2</sub> waveguide to be similar to the input silicon waveguide, which mainly distributes in the waveguide center where the VO<sub>2</sub> layer is laid as shown in Fig. 1(c). Due to low absorption of insulating VO<sub>2</sub>, the light propagating along the waveguide experiences negligible attenuation and hence the insertion loss is very low despite of high overlap between VO<sub>2</sub> layer and waveguide power distribution. Once a voltage pulse is applied to the graphene sheets, the modulator switches to the ON-state. Electron injection followed by resistive heating induces the VO<sub>2</sub> phase transition from the insulating state to the lossy conducting state. This changes the power distribution profile of the excited optical mode as shown in Fig. 1(d). This is mainly because the conducting VO<sub>2</sub> behaves like a metal with high absorption and reminds us a plasmonic propagation [37]. A portion of power directly interacts with the conducting VO<sub>2</sub> layer and the rest pushes into side layers in vertical direction. Consequently, the propagation loss rises significantly, and the output power of the device is reduced. When the voltage is removed, the heat dissipates mainly through graphene at high-speed rate and the VO<sub>2</sub> returns to the insulating state. Therefore, the propagation loss of the structure drops and the output power of the device reaches that of the OFF-state.

### 3. Results and discussions

The performance of the device in term of extinction ratio, insertion loss, power consumption, and modulation speed depends on the VO<sub>2</sub> thickness  $t$ , and hence it should be optimized to achieve the desired operation. So, we sweep the VO<sub>2</sub> thickness  $t$  and the insertion loss of the device in both OFF- and ON-states are plotted in Fig. 2. In the OFF-state, due to the close effective index of input silicon and hybrid Si/VO<sub>2</sub> waveguide, the coupling loss is lower than 0.05 dB (0.2 dB) for VO<sub>2</sub> thickness of  $t = 10$  nm (100 nm) according to our simulations. This implies that the insertion loss mainly dictated by absorption in VO<sub>2</sub> material. However, the proposed modulator possesses negligible OFF-state insertion loss because the VO<sub>2</sub> has a low loss in the insulating phase. With an increase of VO<sub>2</sub> thickness  $t$ , the insertion loss slightly increases since the overlap between the power distribution of waveguide mode and VO<sub>2</sub> layer that is a lossy medium becomes stronger and hence the overall loss increases slightly. On the other hand, in the ON-state, the high absorption of VO<sub>2</sub> in the conducting phase combined with significant coupling loss between input silicon and Si/VO<sub>2</sub> waveguide incur large insertion loss that increases sharply for the thicker

VO<sub>2</sub> layer. As  $t$  increases beyond 60 nm, the insertion loss continues to slightly increase. This can be justified by the power distribution of hybrid Si/VO<sub>2</sub> waveguide. For thick VO<sub>2</sub> thickness, the optical mode of waveguide spreads in vertical directions which causes a significant portion of the power to propagate in the region outside of the lossy VO<sub>2</sub> layer into the substrate and silicon regions.

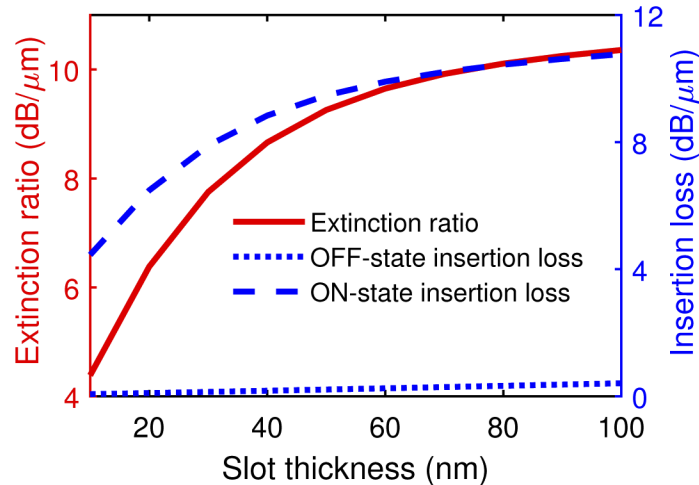


**Fig. 2.** The extinction ratio and insertion losses for both OFF- and ON-states of the proposed modulator as a function of VO<sub>2</sub> slot thickness.

The extinction ratio of the modulator defined as the ratio of the propagation loss when the modulator works in the OFF- (VO<sub>2</sub> Insulation phase) to the ON- (VO<sub>2</sub> conducting phase) state i.e.  $ER = IL_{OFF}/IL_{ON}$  is plotted in Fig. 2. For example, an extinction ratio of  $ER=10.3 \text{ dB}/\mu\text{m}$  can be achieved for VO<sub>2</sub> thickness of  $t = 100 \text{ nm}$  while the corresponding insertion loss is only  $0.43 \text{ dB}/\mu\text{m}$ . For the case of  $t = 10 \text{ nm}$ , the proposed modulator offers an extinction ratio of  $4.4 \text{ dB}/\mu\text{m}$  and insertion loss of only  $0.11 \text{ dB}/\mu\text{m}$ . Compared to the previous mid-IR modulator based on FCD [5,6], and thermo-optic effect [8] the length of the device reduces orders of magnitude with similar extinction ratio while the insertion loss also decreases. Also, it is worth noting that the resulted extinction ratio is among the highest value in comparison with that of the previous reports using phase change materials while our insertion loss is much lower [13]. It should be noted that the proposed device can work in the near-IR wavelength regime as well. Our simulations show an extinction ratio of  $ER = 9 \text{ dB}/\mu\text{m}$  with an insertion loss of  $1.6 \text{ dB}/\mu\text{m}$  at  $\lambda = 1.55 \mu\text{m}$  for VO<sub>2</sub> thickness of  $t = 100 \text{ nm}$  embedded in a redesigned launching silicon waveguide with  $450 \times 220 \text{ nm}^2$  cross-section, using the refractive index of incorporated material at  $\lambda = 1.55 \mu\text{m}$ .

For further understanding the operation of the proposed device, Fig. 3 shows the top view of the power intensity along the propagation direction of the device for a fundamental quasi-TE mode of input silicon waveguide when VO<sub>2</sub> is in the insulating and conducting phases, respectively. The device length and VO<sub>2</sub> layer thicknesses are  $L = 1 \mu\text{m}$  and  $t = 50 \text{ nm}$ , respectively. In OFF-state, light travels through the device with a negligible insertion loss of 0.3 dB as the VO<sub>2</sub> is in the insulating phase. By switching the VO<sub>2</sub> phase to conducting corresponding ON-state, the light decays strongly during the propagation along the device.

The wavelength-dependent operation of a modulator is an important parameter. For this reason, the extinction ratio and OFF-state insertion loss of the device as a function of wavelength for different VO<sub>2</sub> thicknesses  $t$  are plotted in Fig. 4. Along with the increase of wavelength, the OFF state insertion loss remains nearly unchanged while extinction ratio declines slightly. In the

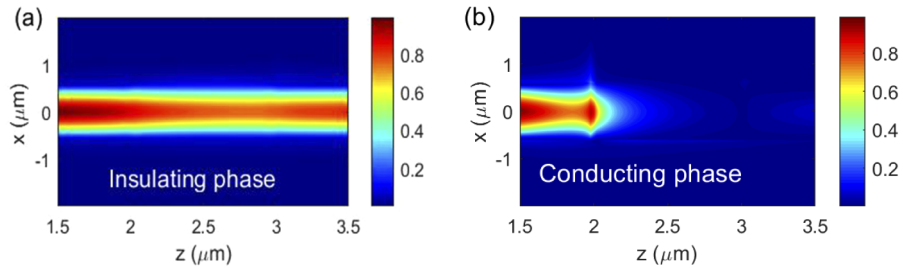


**Fig. 3.** The top view of the power intensity along the propagation direction of proposed modulator for VO<sub>2</sub> is in (a) insulating phase and (b) conducting phase, where  $L = 1\ \mu\text{m}$  and  $t = 50\ \text{nm}$ .

entire wavelength range of  $3.7\ \mu\text{m}$  to  $3.9\ \mu\text{m}$ , the extinction ratio is larger than  $10\ \text{dB}/\mu\text{m}$  ( $4.2\ \text{dB}/\mu\text{m}$ ) for  $t = 100\ \text{nm}$  ( $10\ \text{nm}$ ) which shows only  $0.6\ \text{dB}/\mu\text{m}$  ( $0.3\ \text{dB}/\mu\text{m}$ ) drop compared to the best extinction ratio of the proposed device at given wavelength spectrum. This indicates the proposed device supports broadband spectral operation.

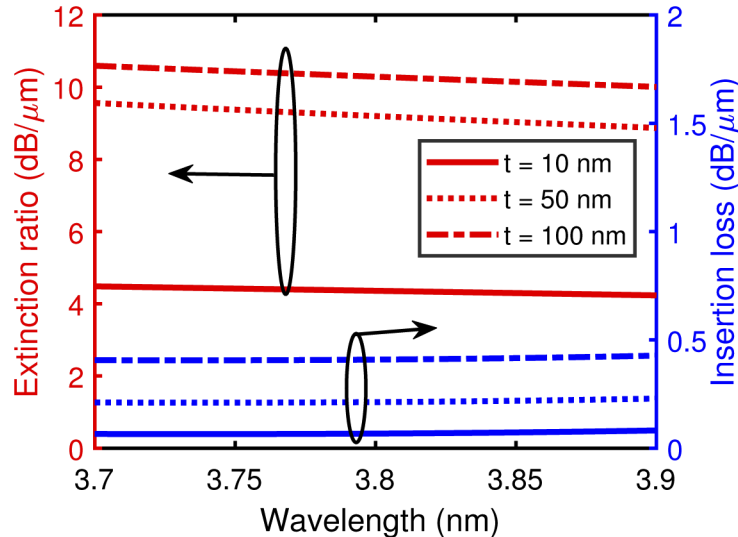


**Fig. 4.** The extinction ratio and insertion loss of the proposed modulator as a function of wavelength for different VO<sub>2</sub> thickness  $t$ .

Apart from extinction ratio and insertion loss, modulation speed and energy consumption are vital and important in addition to parameters for estimating the performance of the proposed modulator. The speed of the proposed structure is determined by VO<sub>2</sub> phase transition speed and  $RC$  response time of the structure. The capacitance  $C$  can be approximately estimated from a simple parallel plate capacitor model (formed by the VO<sub>2</sub> layer as a dielectric sandwiched between two graphene electrodes acting as two conductive plates). The total structure resistance  $R$  consisting of graphene sheet resistance  $R_s$  and Ti-Au/graphene contact resistance  $R_c$ , which can be calculated by  $R = R_s + R_c = (R_s d + 2R_c)/L$ . Here, in our calculation  $R_s = 200\ \Omega/\square$  and  $R_c = 100\ \Omega\cdot\mu\text{m}$  were used [29]. According to our calculations, the  $RC$  response time of the modulator is estimated as  $\tau = 0.12/t$  (ps·nm). This indicates that the  $RC$  response time is in the range of the picosecond scale and therefore does not restrict the modulation speed considering the nanosecond range of VO<sub>2</sub> transition time. To estimate the speed of the VO<sub>2</sub> phase transition,

a thermal simulation using finite-element-method (FEM) is conducted to solve the heat transfer equation and current flow equations. In our simulations, the used thermal properties of materials including VO<sub>2</sub>, SiO<sub>2</sub>, and Si are provided in Table 1. Graphene is treated as a 0.34 nm layer with thermal conductivity, heat capacity, and density given in Table 1. Also, the heat conversion coefficient of air is set to be 10 W/m<sup>2</sup>K [28].

To change the phase of VO<sub>2</sub> from insulator to metal, a proper voltage pulse providing an electric field stronger than that of threshold  $6.5 \times 10^7$  V/m is applied to the VO<sub>2</sub> layer by graphene contacts. This causes carriers to inject to the insulating VO<sub>2</sub> layer via the electronic process of the Poole-Frenkel mechanism [20,38] leading to rapid heating and formation of a current path in the VO<sub>2</sub> layer between the graphene contacts. After that, the electric field drops and the current flows through it that causes a joule heating process and extends the metaled volume of VO<sub>2</sub>. Figure 4 plots the temperature of the VO<sub>2</sub> layer as a function of time for different  $t$  and  $L = 1 \mu\text{m}$ . The required electric field is achieved with voltages of 0.65 V, 3.25 V and 6.5 V with a duration of 6 ns for a VO<sub>2</sub> thickness of  $t = 10$  nm, 50 nm, and 100 nm, respectively. One can see that the heat up process time increases for the thicker VO<sub>2</sub> layer because the larger volume VO<sub>2</sub> needs more energy for the phase transition. For  $t = 10$  nm, only 6 ns takes to reach temperature of about 68°C which indicates a fast dynamic response for phase transitions.

This result is much less than other results exploiting Joule heating with lower input power [13,16,18]. Figure 6 depicts the spatial temperature distribution of the proposed modulator at 6 ns after applying power for  $t = 10$  nm and  $L = 1 \mu\text{m}$ . The temperature of the VO<sub>2</sub> layer rises to above 68°C that ensures the phase transition is induced by heat. Note that the temperature in graphene regions in contact with the VO<sub>2</sub> is lower than that of the other regions due to instant heat transfer to the VO<sub>2</sub> layer at a faster rate. More details can also be seen clearly from temperature distributions in the cross-sections along cut lines (cut 1 and cut 2) as shown in Fig. 6(b) and (c). At the end of the pulse duration, the modulator switches from the ON- to OFF- state and the VO<sub>2</sub> transfers back to the insulating state with a delay. According to Fig. 5, as expected, the required time for the reverse phase transition from conducting to insulating is longer than that of the insulator to conducting transition. However, it occurs very faster than the other reported response times for the electrical actuation of the VO<sub>2</sub> [13,16,19]. For example, the reverse transition time is only about 17 ns for  $t = 10$  nm. Because of the huge thermal conductivity of graphene, it draws the heat of the VO<sub>2</sub> layer at high-speed rate and then the VO<sub>2</sub> temperature reduces to below of the threshold value rapidly, which leads to a phase transition to the insulating state. With the

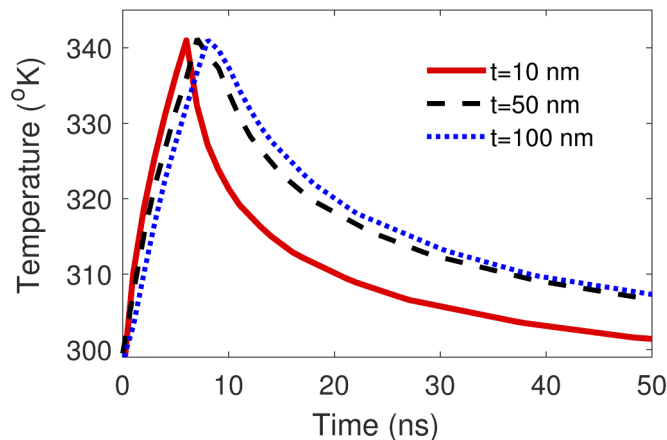


**Fig. 5.** Temperature in the VO<sub>2</sub> layer as a function of time for different VO<sub>2</sub> thicknesses  $t$ , where  $L = 1 \mu\text{m}$  and 1.5-mW heating power.

increase of the VO<sub>2</sub> layer thickness  $t$ , the recovery time becomes longer. Because thicker VO<sub>2</sub> layers require more energy for transition and thus the dissipation time is longer.

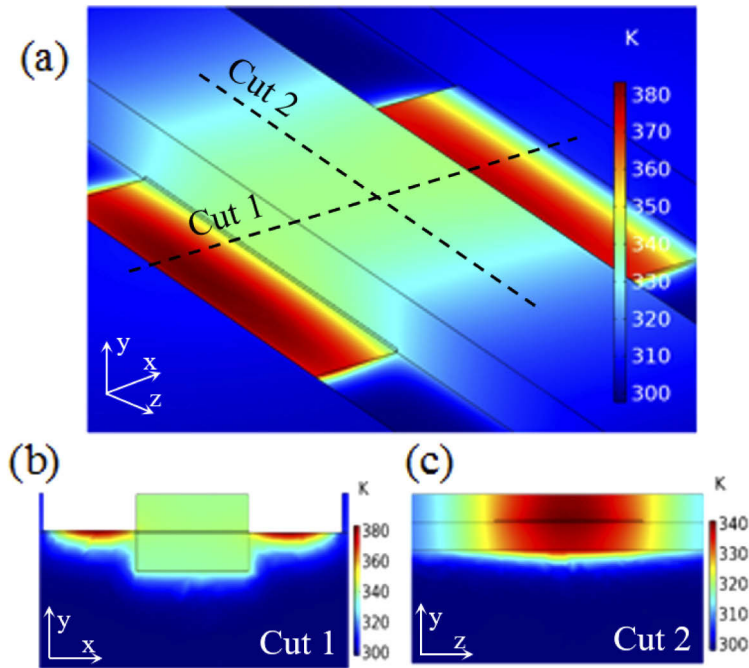


**Fig. 6.** (a) Three-dimension spatial temperature distribution of the heated hybrid Si/VO<sub>2</sub> structure induced by graphene microheater. (b) and (c) Temperature distribution for the cross sections along Cut 1 and Cut 2, respectively, for a heating power of 1.5 mW at 6 ns after applying power and  $t = 10$  nm, and  $L = 1$   $\mu$ m.

It should be noted that the heating process of the VO<sub>2</sub> layer also increases the temperature of the other regions of the structure including Si, SiO<sub>2</sub> and graphene sheets. However, in the working temperature range, the proposed structure is not sensitive to the variations of the refractive index of the Si and SiO<sub>2</sub> and hence the achieved results changes are ignorable. Also, the conductivity of graphene varies slightly when the temperature increases [30] so that the results remain approximately unchanged. Note that the modulation speed of the proposed modulator can be further improved by the combination of our proposal presented in this paper with a four-level pulse amplitude method, which is well-argued in [19].

The most challenging part in realizing our designed structure is to obtain a good VO<sub>2</sub> performance deposited on the graphene layer. Recently, VO<sub>2</sub> material has been successfully deposited on the graphene layer so it is possible to experimentally realize our proposed structure [39]. However, it is well known that the properties of VO<sub>2</sub> depend on the substrate, thickness, and other fabrication parameters [14,16,31,40,41]. This potentially causes a deviation in the overall performance of the modulator. Our simulations show that the sensitivity of the modulator to optical properties and uncertainties is low and not has a significant effect. Note that the prior works demonstrated that the thermal conductivity of non-suspended graphene lies between 2000–4000 W/mK [28,36,42]. Guided by this point, in the manuscript, a mean thermal conductivity of 3000 W/mK is considered.

#### 4. Conclusion

In conclusion, optical and thermal designation of a high-speed ultra-compact mid-IR hybrid Si/VO<sub>2</sub> modulator in the form of a vertical Si-graphene-VO<sub>2</sub>-graphene-Si vertical stack layer, is proposed and analyzed in this paper. Extraordinary electrical and thermal properties of graphene motivate to use it as electrodes for two reasons: 1) its electrical properties are used to electrically trigger a phase transition in the VO<sub>2</sub> layer. 2) The high thermal conductivity helps the heating and dissipation process and hence significantly improves the modulation speed. The presented numerical simulations show a low rise time  $\approx 6$  ns and fall time  $\approx 17$  ns for the proposed modulator with an extinction ratio of 4.4 dB/ $\mu\text{m}$  and very low insertion loss of 0.1 dB/m. According to our calculations, the proposed modulator provides higher modulation speed compared to the previously reported VO<sub>2</sub>-based optical modulator.

#### Disclosures

The authors declare no conflicts of interest.

#### References

1. G. Z. Mashanovich, F. Y. Gardes, D. J. Thomson, Y. Hu, K. Li, M. Nedeljkovic, J. Soler Penades, A. Z. Khokhar, C. J. Mitchell, S. Stankovic, R. Topley, S. A. Reynolds, Y. Wang, B. Troia, V. M. N. Passaro, C. G. Littlejohns, T. Dominguez Bucio, P. R. Wilson, and G. T. Reed, "Silicon photonic waveguides and devices for near-and mid-ir applications," *IEEE J. Sel. Top. Quantum Electron.* **21**(4), 407–418 (2015).
2. Y. Zou, S. Chakravarty, C.-J. Chung, X. Xu, and R. T. Chen, "Mid-infrared silicon photonic waveguides and devices," *Photonics Res.* **6**(4), 254–276 (2018).
3. V. M. Lavchiev and B. Jakoby, "Photonics in the mid-infrared: Challenges in single-chip integration and absorption sensing," *IEEE J. Sel. Top. Quantum Electron.* **23**(2), 452–463 (2017).
4. T. Hu, B. Dong, X. Luo, T.-Y. Liow, J. Song, C. Lee, and G.-Q. Lo, "Silicon photonic platforms for mid-infrared applications," *Photonics Res.* **5**(5), 417–430 (2017).
5. T. Li, M. Nedeljkovic, N. Hattasan, W. Cao, Z. Qu, C. G. Littlejohns, J. S. Penades, L. Mastronardi, V. Mittal, D. Benedikovic, D. J. Thomson, F. Y. Gardes, H. Wu, Z. Zhou, and G. Z. Mashanovich, "Ge-on-Si modulators operating at mid-infrared wavelengths up to 8  $\mu\text{m}$ ," *Photonics Res.* **7**(8), 828–836 (2019).
6. M. Nedeljkovic, C. G. Littlejohns, A. Z. Khokhar, M. Banakar, W. Cao, J. S. Penades, D. T. Tran, F. Y. Gardes, D. J. Thomson, G. T. Reed, H. Wang, and G. Z. Mashanovich, "Silicon-on-insulator free-carrier injection modulators for the mid-infrared," *Opt. Lett.* **44**(4), 915–918 (2019).
7. M. A. Richardson and J. A. Coath, "Infrared optical modulators for missile testing," *Opt. Laser Technol.* **30**(2), 137–140 (1998).
8. M. Nedeljkovic, S. Stanković, C. J. Mitchell, A. Z. Khokhar, S. A. Reynolds, D. J. Thomson, F. Y. Gardes, C. G. Littlejohns, G. T. Reed, and G. Z. Mashanovich, "Mid-infrared thermo-optic modulators in SOI," *IEEE Photonics Technol. Lett.* **26**(13), 1352–1355 (2014).
9. M. A. Van Camp, S. Assefa, D. M. Gill, T. Barwicz, S. M. Shank, P. M. Rice, T. Topuria, and W. M. Green, "Demonstration of electrooptic modulation at 2165 nm using a silicon mach-zehnder interferometer," *Opt. Express* **20**(27), 28009–28016 (2012).
10. M. Nedeljkovic, R. Soref, and G. Z. Mashanovich, "Free-carrier electrorefraction and electroabsorption modulation predictions for silicon over the 1–14  $\mu\text{m}$  infrared wavelength range," *IEEE Photonics J.* **3**(6), 1171–1180 (2011).
11. Q. Xu, S. Manipatruni, B. Schmidt, J. Shakya, and M. Lipson, "12.5 Gbits/s carrier-injection-based silicon micro-ring silicon modulators," *Opt. Express* **15**(2), 430–436 (2007).
12. S. Manipatruni, R. K. Dokania, B. Schmidt, N. Sherwood-Droz, C. B. Poitras, A. B. Apsel, and M. Lipson, "Wide temperature range operation of micrometer-scale silicon electro-optic modulators," *Opt. Lett.* **33**(19), 2185–2187 (2008).
13. K. J. Miller, R. F. Haglund, and S. M. Weiss, "Optical phase change materials in integrated silicon photonic devices," *Opt. Mater. Express* **8**(8), 2415–2429 (2018).
14. R. M. Briggs, I. M. Pryce, and H. A. Atwater, "Compact silicon photonic waveguide modulator based on the vanadium dioxide metal-insulator phase transition," *Opt. Express* **18**(11), 11192–11201 (2010).
15. K. J. Miller, K. A. Hallman, R. F. Haglund, and S. M. Weiss, "Silicon waveguide optical switch with embedded phase change material," *Opt. Express* **25**(22), 26527–26536 (2017).
16. A. Joushaghani, J. Jeong, S. Paradis, D. Alain, J. S. Aitchison, and J. K. Poon, "Wavelength-size hybrid Si-VO<sub>2</sub> waveguide electroabsorption optical switches and photodetectors," *Opt. Express* **23**(3), 3657–3668 (2015).
17. B. Janjan, M. Miri, A. Zarifkar, and M. Heidari, "Design and simulation of compact optical modulators and switches based on Si-VO<sub>2</sub>-Si horizontal slot waveguides," *J. Lightwave Technol.* **35**(14), 3020–3028 (2017).

18. K. J. Miller, P. Markov, R. E. Marvel, R. F. Haglund, and S. M. Weiss, "Hybrid silicon-vanadium dioxide electro-optic modulators," *Proc. SPIE* **9752**, 975203 (2016).
19. S. Mohammadi-Pouyan, M. Miri, and M. H. Sheikhi, "Design of a vanadium dioxide-based dual-polarization optical pam4 modulator," *J. Opt. Soc. Am. B* **35**(12), 3094–3103 (2018).
20. P. Markov, R. E. Marvel, H. J. Conley, K. J. Miller, R. F. Haglund Jr, and S. M. Weiss, "Optically monitored electrical switching in VO<sub>2</sub>," *ACS Photonics* **2**(8), 1175–1182 (2015).
21. F. Bonaccorso, Z. Sun, T. Hasan, and A. Ferrari, "Graphene photonics and optoelectronics," *Nat. Photonics* **4**(9), 611–622 (2010).
22. A. Grigorenko, M. Polini, and K. Novoselov, "Graphene plasmonics," *Nat. Photonics* **6**(11), 749–758 (2012).
23. Q. Bao and K. P. Loh, "Graphene photonics, plasmonics, and broadband optoelectronic devices," *ACS Nano* **6**(5), 3677–3694 (2012).
24. P. Avouris and M. Freitag, "Graphene photonics, plasmonics, and optoelectronics," *IEEE J. Sel. Top. Quantum Electron.* **20**(1), 72–83 (2014).
25. M. Heidari and V. Ahmadi, "Design and analysis of a graphene magneto-plasmon waveguide for plasmonic mode switch," *IEEE Access* **7**, 43406–43413 (2019).
26. A. A. Balandin, S. Ghosh, W. Bao, I. Calizo, D. Teweldebrhan, F. Miao, and C. N. Lau, "Superior thermal conductivity of single-layer graphene," *Nano Lett.* **8**(3), 902–907 (2008).
27. S. Yan, X. Zhu, L. H. Frandsen, S. Xiao, N. A. Mortensen, J. Dong, and Y. Ding, "Slow-light-enhanced energy efficiency for graphene microheaters on silicon photonic crystal waveguides," *Nat. Commun.* **8**(1), 14411 (2017).
28. S. Gan, C. Cheng, Y. Zhan, B. Huang, X. Gan, S. Li, S. Lin, X. Li, J. Zhao, H. Chen, and Q. Bao, "A highly efficient thermo-optic microring modulator assisted by graphene," *Nanoscale* **7**(47), 20249–20255 (2015).
29. F. Giubileo and A. Di Bartolomeo, "The role of contact resistance in graphene field-effect devices," *Prog. Surf. Sci.* **92**(3), 143–175 (2017).
30. Y. Francescato, V. Giannini, and S. A. Maier, "Strongly confined gap plasmon modes in graphene sandwiches and graphene-on-silicon," *New J. Phys.* **15**(6), 063020 (2013).
31. C. Wan, Z. Zhang, D. Woolf, C. M. Hessel, J. Rensberg, J. M. Hensley, Y. Xiao, A. Shahsafi, J. Salman, S. Richter, Y. Sun, M. M. Qazilbash, R. Schmidt-Grund, C. Ronning, S. Ramanathan, and M. A. Kats, "On the optical properties of thin-film vanadium dioxide from the visible to the far infrared," *Ann. Phys.* **531**(10), 1900188 (2019).
32. G. Chandrashekar, H. Barros, and J. Honig, "Heat capacity of VO<sub>2</sub> single crystals," *Mater. Res. Bull.* **8**(4), 369–374 (1973).
33. D.-W. Oh, C. Ko, S. Ramanathan, and D. G. Cahill, "Thermal conductivity and dynamic heat capacity across the metal-insulator transition in thin film VO<sub>2</sub>," *Appl. Phys. Lett.* **96**(15), 151906 (2010).
34. E. D. Palik, *Handbook of Optical Constants of Solids*, vol. 3 (Academic Press, 1998).
35. S. Moon, M. Hatano, M. Lee, and C. P. Grigoropoulos, "Thermal conductivity of amorphous silicon thin films," *Int. J. Heat Mass Transfer* **45**(12), 2439–2447 (2002).
36. J. T. Kim, K. H. Chung, and C.-G. Choi, "Thermo-optic mode extinction modulator based on graphene plasmonic waveguide," *Opt. Express* **21**(13), 15280–15286 (2013).
37. D. K. Gramotnev and S. I. Bozhevolnyi, "Plasmonics beyond the diffraction limit," *Nat. Photonics* **4**(2), 83–91 (2010).
38. J. S. Brockman, L. Gao, B. Hughes, C. T. Rettner, M. G. Samant, K. P. Roche, and S. S. P. Parkin, "Subnanosecond incubation times for electric-field-induced metallization of a correlated electron oxide," *Nat. Nanotechnol.* **9**(6), 453–458 (2014).
39. H. Kim, Y. Kim, T. Kim, A.-R. Jang, H. Y. Jeong, S. H. Han, D. H. Yoon, H. S. Shin, D. J. Bae, K. S. Kim, and W. S. Yang, "Enhanced optical response of hybridized VO<sub>2</sub>/graphene films," *Nanoscale* **5**(7), 2632–2636 (2013).
40. J. K. Kana, J. Ndjaka, G. Vignaud, A. Gibaud, and M. Maaza, "Thermally tunable optical constants of vanadium dioxide thin films measured by spectroscopic ellipsometry," *Opt. Commun.* **284**(3), 807–812 (2011).
41. H. W. Verleur, A. S. Barker, and C. N. Berglund, "Optical properties of VO<sub>2</sub> between 0.25 and 5 eV," *Phys. Rev.* **172**(3), 788–798 (1968).
42. L. Yu, Y. Yin, Y. Shi, D. Dai, and S. He, "Thermally tunable silicon photonic microdisk resonator with transparent graphene nanoheaters," *Optica* **3**(2), 159–166 (2016).